

# Origins of Anomalous Transport in Disordered Media: Structural and Dynamic Controls

Yaniv Edery<sup>1</sup>, Harvey Scher<sup>1</sup>, Alberto Guadagnini<sup>2</sup> and Brian Berkowitz<sup>1</sup>

1. *Department of Environmental Sciences and Energy Research,  
Weizmann Institute of Science, 76100 Rehovot, Israel*

2. (a) *Dipartimento di Ingegneria Civile e Ambientale,  
Politecnico di Milano, 20133 Milano, Piazza L. Da Vinci 32,  
Italy* (b) *Department of Hydrology and Water Resources,  
University of Arizona, Tucson, Arizona 85721, USA*

We quantitatively identify the origin of anomalous transport in a representative model of a heterogeneous system—tracer migration in the complex flow patterns of a lognormally distributed hydraulic conductivity ( $K$ ) field. The transport, determined by a particle tracking technique, is characterized by breakthrough curves; the ensemble averaged curves document anomalous transport in this system, which is entirely accounted for by a truncated power-law distribution of local transition times  $\psi(t)$  within the framework of a continuous time random walk. Unique to this study is the linking of  $\psi(t)$  directly to the system heterogeneity. We assess the statistics of the dominant preferred pathways by forming a particle-visitation weighted histogram  $\{wK\}$ . Converting the  $\ln(K)$  dependence of  $\{wK\}$  into time yields the equivalence of  $\{wK\}$  and  $\psi(t)$ , and shows the part of  $\{wK\}$  that forms the power-law of  $\psi(t)$ , which is the origin of anomalous transport. We also derive an expression defining the power law exponent in terms of the  $\{wK\}$  parameters. This equivalence is a remarkable result, particularly given the correlated  $K$ -field, the complexity of the flow field and the statistics of the particle transitions.

PACS numbers:

Anomalous transport was first discovered in the electron transport of amorphous semiconductors [1]. Such behavior is now recognized to be ubiquitous in a broad range of physical processes: chemical transport in porous and fractured geological formations [2–6], diffusion of mRNA [7] and chromosomal loci in live cells [8], and tracer movement in micro-organism suspensions [9], crowded fluids [10], gels [11] and porous media as affected by biofilm growth [12]. Anomalous transport in disordered media is manifested by nonlinear time dependence of the particle displacement mean,  $\bar{\ell} \propto t^\beta$ , and  $\bar{\ell}/\text{rms} = \text{const}$  for  $\beta < 1$  (with rms the root mean square particle displacement), as well as by long tails in the spatial and temporal distributions of particles.

As noted in many of these studies, the mechanisms for anomalous transport and diffusion are varied, e.g., flow in heterogeneous fracture networks and porous media, multiple trapping, chemical sorption, migration in crowded environments and electron transfer (hopping), and yet the time dependence is the same. In this Letter, the origins of anomalous transport are identified through an analysis of the particle pathway statistics in a completely controllable model disordered geophysical system. We show the transport cannot be explained solely by the structural knowledge of the disordered medium. We probe the nuanced dynamic processes and find that the basic determinant of the distribution of local transition times, which defines the anomalous transport, is a conductivity histogram weighted by the particle flux. This remarkable relationship is quantitatively exact.

The system is a geophysical model, based on a log-normally distributed and spatially correlated hydraulic

conductivity ( $K$ ) random field in a fluid saturated, two-dimensional (2D) domain. The field is characterized by a variance of  $\ln(K)$ ,  $\sigma^2$ . We determine the steady-state uniform (in the mean) flow and the transport of tracer particles through it as a function of head gradients and  $\sigma^2$ . The transport, determined by a particle tracking technique, is characterized by breakthrough curves (BTCs), quantifying the arrival of an injected plume of particles at the domain outlet. The ensemble averaged BTC for this disordered system documents anomalous (or “non-Fickian”) transport. Other studies have attempted to quantify the effect of the underlying heterogeneous structure of the  $K$  distribution on BTC patterns; they note the occurrence of preferential flow paths and long BTC tails, but quantification of the relationship between  $K$  field statistics and transport parameters remains obscure [e.g., 13, 14]. Here, not only is it shown that anomalous behavior is accounted for within the theoretical framework of a continuous time random walk (CTRW), but an entirely new assessment—the statistical analysis of flux-weighted particle pathways—is linked directly to the CTRW framework.

The discrete (in space), temporal semi-Markov CTRW transport equations leads to the (Laplace space) working continuum transport equation for the normalized concentration  $c(\mathbf{s}, t)$  for an ensemble-averaged system:

$$u\tilde{c}(\mathbf{s}, u) - c_0(\mathbf{s}) = -\tilde{M}(u)[\mathbf{v}_\psi \cdot \nabla \tilde{c}(\mathbf{s}, u) - \mathbf{D}_\psi : \nabla \nabla \tilde{c}(\mathbf{s}, u)] \quad (1)$$

where  $\tilde{M}(u) \equiv \bar{t}u\tilde{\psi}(u)/[1 - \tilde{\psi}(u)]$  is a memory function, with the Laplace transform of a function  $f(t)$  denoted by  $\tilde{f}(u)$ ,  $\bar{t}$  is a characteristic time,  $\psi(t)$  is the probability rate

for a transition time  $t$  between sites, and  $\bar{t}\mathbf{v}_\psi$  and  $\bar{t}\mathbf{D}_\psi$  are, respectively, the first and second moments of  $p(\mathbf{s})$ , the probability distribution of the length of the transitions. The “transport velocity”,  $\mathbf{v}_\psi$ , is distinct from the “average fluid velocity”,  $\mathbf{v}$ , due to the heterogeneity.

Unique to this study is the linking of  $\psi(t)$  directly to the heterogeneity of our model system. The key feature of the CTRW distribution  $\psi(t)$  that we use, which has been successful in analyzing a number of laboratory and field observations, is a truncated power law (TPL) distribution of the site-to-site transition times with an evolution to Fickian behavior:

$$\psi(t) = \frac{n}{t_1} \exp(-t/t_2) / (1 + t/t_1)^{1+\beta} \quad (2)$$

where  $n \equiv (t_1/t_2)^{-\beta} \exp(-t_1/t_2) / \Gamma(-\beta, t_1/t_2)$  is a normalization factor (for large  $t_2$ ,  $n \approx \beta$  [15]),  $\beta$  is a measure of the transition time spectrum,  $t_1$  ( $= \bar{t}$  in (1)) is a characteristic time, e.g., for median transitions between sites,  $t_2$  is a “cutoff” time, and  $\Gamma(a, x)$  is the incomplete Gamma function [16]. For transition times  $t_1 < t < t_2$ ,  $\psi(t)$  behaves as a power law  $\propto (t/t_1)^{-1-\beta}$  while for  $t > t_2$ ,  $\psi(t)$  decreases exponentially; thus a finite  $t_2$  enables evolution from non-Fickian to Fickian transport. A pure exponential  $\psi(t) = \lambda \exp(-\lambda t)$  reduces the CTRW transport equation (1) to the advection-dispersion equation (ADE):  $\partial c(\mathbf{s}, t) / \partial t = -\mathbf{v}(\mathbf{s}) \cdot \nabla c(\mathbf{s}, t) + \nabla \cdot \nabla(\mathbf{D}(\mathbf{s})c(\mathbf{s}, t))$  where  $\mathbf{v}(\mathbf{s})$  is the velocity field and  $\mathbf{D}(\mathbf{s})$  is the dispersion tensor. The basic question now is: what aspects of the interplay between the detailed particle dynamics and the structural features of the  $K$ -field give rise to (2)?

As background to answer this question, our method of model construction and particle tracking is outlined in the Supplementary Material (SM) [17]. The BTC is a key measure of the accumulative response of all the transitions comprising the transport within the velocity field of the domain. The ensemble mean BTCs (100 realizations) are seen in Fig. 1, with  $\sigma^2 = 3, 5, 7$ , and fits with 1D solutions of the CTRW (using (2)) and the ADE. The distinguishing feature is the broadness of the BTCs, which increases with increasing  $\sigma^2$ . Overall, the CTRW effectively captures the tails as well as the peaks of the BTCs. The TPL values of  $\beta$  show a clear trend to decrease (from 1.77 to 1.57) with increasing  $\sigma^2$  (3 to 7), as expected. This emphasizes the physical meaning of  $\beta$ : it is a generalized dispersion parameter that captures the entire shape of the BTC and not only a width of a normal curve (i.e.,  $\mathbf{D}$ ). The subtle interplay among the TPL parameters  $\beta, t_1, t_2$ , which determine the shape of the entire TPL, is quantified in terms of the particle paths (below).

Fig. 2a shows the heterogeneity of the  $K$ -field with  $\sigma^2 = 5$ . The mean  $\ln(K)$  is 0 with a 7 decade spread in  $K$  over a statistically homogeneous map of a single realization. The lowest values of  $\ln(K)$  tend to appear as local patches with a concentric ring of moderately lower conductivity. We investigate how this map manifests the preferred particle pathways. As a reference, Fig. 2b shows a

path constructed by excluding cells where the conductivity is lower than a given threshold; the threshold value is lowered iteratively until a connected (percolation) path is formed. This type of critical path analysis (CPA) [18, 19] has been linked, using percolation theory scaling arguments, to anomalous transport and CTRW theory [20–22]. In Fig. 2c, we superimpose on the full conductivity field (Fig. 2a) the number of particles visiting each cell. The striking feature that emerges is the occurrence of preferential particle paths which are so dominant that the difference in particle visitation in various cells ranges from zero to 10% of the total number of particles in the simulation. The white areas where particles do not enter have an effect on the surrounding areas, confining the preferential paths to converge between low conductivity areas.

Figure 2d shows a sparser set of preferential paths than Fig. 2c, generated by recording only those cells having visitations of  $\geq 100$  particles (0.1% of all particles). The color contrasts show an admixture of the higher conductivities in the paths, however low conductivity cells are still present. We find (not shown) that as residence time increases (i.e., for smaller head gradients), the overall transport evolves to a biased Gaussian (denoting Fickian) behavior for time scales  $> t_2$ , with a BTC described by the ADE (see Fig. 1). Significantly, though, the particle flux in this limit is not spatially uniform across the domain cross sections, as commonly envisaged for application of the ADE; rather, the flux is still, largely, in limited preferential pathways. It is illuminating to observe deviations from the particle pathways defined by the CPA. Fig. 2e shows the “lower conductivity transitions” (LCTs) — defined for convenience as cells with  $K$  values less than the CPA threshold — taken from the paths in Fig. 2d. Clearly, the critical path is insufficient to predict or estimate the actual particle movement. Indeed, CPA and percolation scaling arguments, based entirely on the  $K$  field structure [22], do not include the significant influence of the transitions below the threshold and residence time effects (see below).

Two histograms are shown in Fig. 3, together with a quantitative measure of the LCTs. One histogram corresponds to the conductivity field in Fig. 2a, while the other derives from the preferred paths of Fig. 2c weighted by the particle visitation in each cell, which we designate  $\{wK\}$ . The mean and skewness of  $\{wK\}$  are significantly larger than those for the full  $K$  field (Fig. 3 caption). The mean of  $\{wK\}$  is a quantitative measure of the particle selectivity of the higher conductivity cells. The fraction of the weighted conductivities considered as LCT is 11.5%. Hence these LCTs are significant, and as we show below, are responsible for the long tail in the BTC. The  $\{wK\}$  in Fig. 3 is for one realization; averaging the weighted mean over 100 realizations for the same  $\sigma^2$  follows this pattern closely. Moreover, similar behavior was observed for a variety of realizations with different  $\ln(K)$  variances (see below).

The  $\{wK\}$  is the basic characterization of transport in

our model. This is seen clearly by converting the  $\ln(K)$  axis to time  $t$ . Based on Fig. 3, for each  $K$  bin, we determined the head gradient over each associated cell, and obtained an average head gradient (weighted by the relative number of particles passing through these cells). We then determined the average residence time in these cells, using Darcy's law for flow,  $\Delta t = \theta(\Delta x)^2/(K\Delta h)$ , where  $\theta$  is porosity ( $= 0.3$ ) and  $\Delta h$  is the weighted average head difference over the cell. Determining these average times for cells in all  $K$  bins, we obtain a frequency (weighted by the number of particles) of particle residence times in all cells in the domain. Dividing by  $\Delta t$  to obtain equal bin sizes, yields the probability density result for an ensemble of 100 realizations is shown in Fig. 4; the entire density is coincident with the TPL (2) using  $\beta = 1.63$ . Significantly, the  $\beta$ ,  $t_1$  and  $t_2$  values of (2) used here are the same as those used to determine the BTC in Fig. 1 ( $\sigma^2 = 5$ ). The statistical analysis of particle paths, which renders the probability density  $\{wK\}$ , leads directly to the CTRW framework of the probability density  $\psi(t)$ ; indeed, they are the same. The red portion of the curve corresponds to the power-law region; by equating the logarithmic derivatives of both curves we can develop an analytic expression for  $\beta$  in terms of  $\{wK\}$  parameters. We first write  $K = C/t$  (following Darcy's law), the time associated with each  $K$  being the transit time across a “ $K$ -bin”. The points in Fig. 4 are determined from the numerical  $\{wK\}$  for each realization. The mean of the data in Fig. 4 is matched by  $f = n_k \exp[-(\ln K - \mu)^2/(2\sigma^2)]/t$ , where  $\mu$ , the mean of  $\{wK\}$ , is a function of  $\sigma^2$  and the variance of  $\{wK\}$  is  $\approx \sigma^2$  (confirmed numerically);  $n_k$  is a normalization constant. We compute the logarithmic derivative  $d \log f / d \log t$ , and obtain (see SM [17])

$$\beta = (\mu - \ln K)/\sigma^2 \quad (3)$$

by equating it to  $-1/\beta$ , the log derivative of the TPL (2) in the power law region. This result has a slow time dependence for  $\beta$ ; Fig. 4 has some curvature in the power-law region. The value for  $\beta$  is determined near the end of the range of small  $\ln(K)$  (large time). Using representative ensemble values ( $\sigma^2 = 5$ ,  $\mu = 1.5$ ) and choosing  $\ln K = -6.5$  (the low end (large time) of the LCTs in Fig. 3) yields  $\beta = 1.6$  (see Fig. 1).

A picture emerges from the path analysis of high particle flux through the preferred paths, encountering relatively low conductivities (aided by diffusion). The LCTs with highest particle flux occur in or near the preferred

paths. The inclusion of these LCTs in the context of the preferred path template is sufficient to provide to  $\{wK\}$  a power law behavior of  $\psi(t)$ ; this is the origin of non-Fickian transport. This is highlighted in the power-law region  $t_1 < t < t_2$  of Fig. 4; this region corresponds to a  $\ln(K)$  range  $\lesssim -1$  in the LCT region (red bars in Fig. 3). The role of the  $K$  structure is to set up the flow field, which forms the dynamical basis of the preferred paths. It is the range of LCTs within this context that accounts for the anomalous transport, as demonstrated here with the quantitative relation  $\{wK\} \leftrightarrow \psi(t)$ .

In conclusion, we have quantitatively identified the origin of anomalous transport in a richly representative model of a heterogeneous system. We proceeded via two levels. In the first, we determined the BTCs, which are the cumulative particle arrival times (first passage times). The BTCs document the anomalous nature of the transport by the power-law dependence of late times tails. The BTCs were fit with the solutions of the ADE and the CTRW transport equation (1) using a TPL (2) form of  $\psi(t)$ . The TPL accounts for the full shape of the BTCs, with the TPL  $\beta$  parameter decreasing with enhanced disorder (larger  $\sigma^2$ ) as expected. The TPL  $\psi(t)$  hence serves as a characterization of anomalous transport. In the second level, we deeply examined the nature of the particle pathways across the domain and established the dominance of preferred pathways. We assessed the dynamic statistics of these paths by forming a particle-visitation weighted histogram  $\{wK\}$ . We showed that these paths were, mainly, linked high conductivity cells with an important, sparse mix of a relatively small number of LCTs. We converted the  $\ln(K)$  dependence of  $\{wK\}$  into time and demonstrated the equivalence of  $\{wK\}$  and the TPL  $\psi(t)$ . In effect, we show that one can derive the TPL (2) directly from the statistical analysis of the actual particle pathways! We further pinpointed the range of the LCTs as corresponding to the power-law region of the TPL and derived a simple expression (3) for  $\beta$  in terms of  $\sigma^2$  and  $\mu$ . Thus all the information is contained in  $\{wK\}$ —including all correlations in the transitions—and directly yields the values of  $\beta$  as well as  $t_2$ . This is a remarkable result, particularly given the correlated  $K$ -field, the complexity of the flow field and the statistics of the particle transitions.

This research was supported by the Israel Science Foundation (Grant No. 221/11), and by the Israel Water Authority (Grant No. 450056884).

- 
- [1] H. Scher and E. W. Montroll, Phys. Rev. B **12**, 2455 (1975).
  - [2] B. Berkowitz and H. Scher, Phys. Rev. Lett. **79**, 4038 (1997).
  - [3] B. Berkowitz, A. Cortis, M. Dentz, and S. H., Rev. Geophys. **44**, RG2003 (2006).
  - [4] T. Le Borgne, M. Dentz, and J. Carrera, Phys. Rev. Lett.

**101**, 090601 (2008).

- [5] P. K. Kang, M. Dentz, T. Le Borgne, and R. Juanes, Phys. Rev. Lett. **107**, 180602 (2011).
- [6] S. Rubin, I. Dror, and B. Berkowitz, J. Contam. Hydrol. **132**, 28 (2012).
- [7] I. Golding and E. C. Cox, Phys. Rev. Lett. **96**, 098102 (2006).

- [8] S. C. Weber, A. J. Spakowitz, and J. A. Theriot, Phys. Rev. Lett. **104**, 238102 (2010).
- [9] K. C. Leptos, J. S. Guasto, J. P. Gollub, A. I. Pesci, and R. E. Goldstein, Phys. Rev. Lett. **103**, 198103 (2009).
- [10] J. Szymanski and M. Weiss, Phys. Rev. Lett. **103**, 038102 (2009).
- [11] T. Kosztolowicz, K. Dworecki, and S. Mrowczynski, Phys. Rev. Lett. **94**, 170602 (2005).
- [12] J. D. Seymour, J. P. Gage, S. L. Codd, and R. Gerlach, Phys. Rev. Lett. **93**, 198103 (2004).
- [13] M. Willmann, J. Carrera, and X. Sánchez-Vila, Water Resour. Res. **44**, W12437 (2008).
- [14] M. Bianchi, C. Zheng, C. Wilson, G. R. Tick, G. Liu, and S. M. Gorelick, Water Resour. Res. **47**, W05524 (2011).
- [15] B. Berkowitz, S. Emmanuel, and H. Scher, Water Resour. Res. **44**, W03402 (2008).
- [16] M. Abramowitz and I. Stegun, Handbook of Mathematical Functions (Dover Publications, Inc., New York, 1970).
- [17] Supplementary Material.
- [18] V. Ambegaokar, B. I. Halperin, and J. S. Langer, Phys. Rev. B **4**, 2612 (1971).
- [19] S. Kirkpatrick, Phys. Rev. Lett. **27**, 1722 (1971).
- [20] A. G. Hunt, T. E. Skinner, R. P. Ewing, and B. Ghanbarian-Alavijeh, Eur. Phys. J. B **80**, 411 (2011).
- [21] B. Ghanbarian-Alavijeh, T. E. Skinner, and A. G. Hunt, Phys. Rev. E **86**, 066316 (2012).
- [22] M. Sahimi, Phys. Rev. E **85**, 016316 (2012).

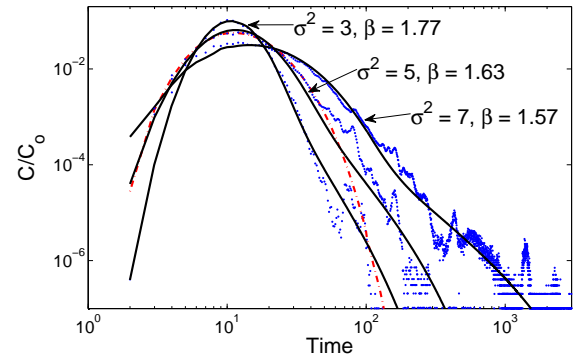


FIG. 1: (Color online) Ensemble breakthrough curves (points) for three  $\ln(K)$  variances ( $\sigma^2 = 3, 5, 7$ ) and a head gradient of 100, and corresponding CTRW fits (curves), with values of  $v_\psi$ ,  $D_\psi$ ,  $\beta$ ,  $t_1$ ,  $t_2$  in (2) of, respectively, [6.0, 15.8, 1.77, 0.055,  $10^{1.6}$ ], [5.9, 30, 1.63, 0.08,  $10^{2.0}$ ], [3.8, 60, 1.57, 0.063,  $10^{3.0}$ ]. Also shown is a fit of the ADE (dashed-dotted curve, for  $\sigma^2 = 5$  with  $v = 3.4$ ,  $D = 39$ ). For comparison, the average fluid velocity is 5.6. All values are in consistent, arbitrary length and time units. The oscillations in the BTC tails are caused by the formation of a limited set of preferential channels (see Fig. 2 below), leading to variations in the distribution of small numbers of particles arriving at the outlet.



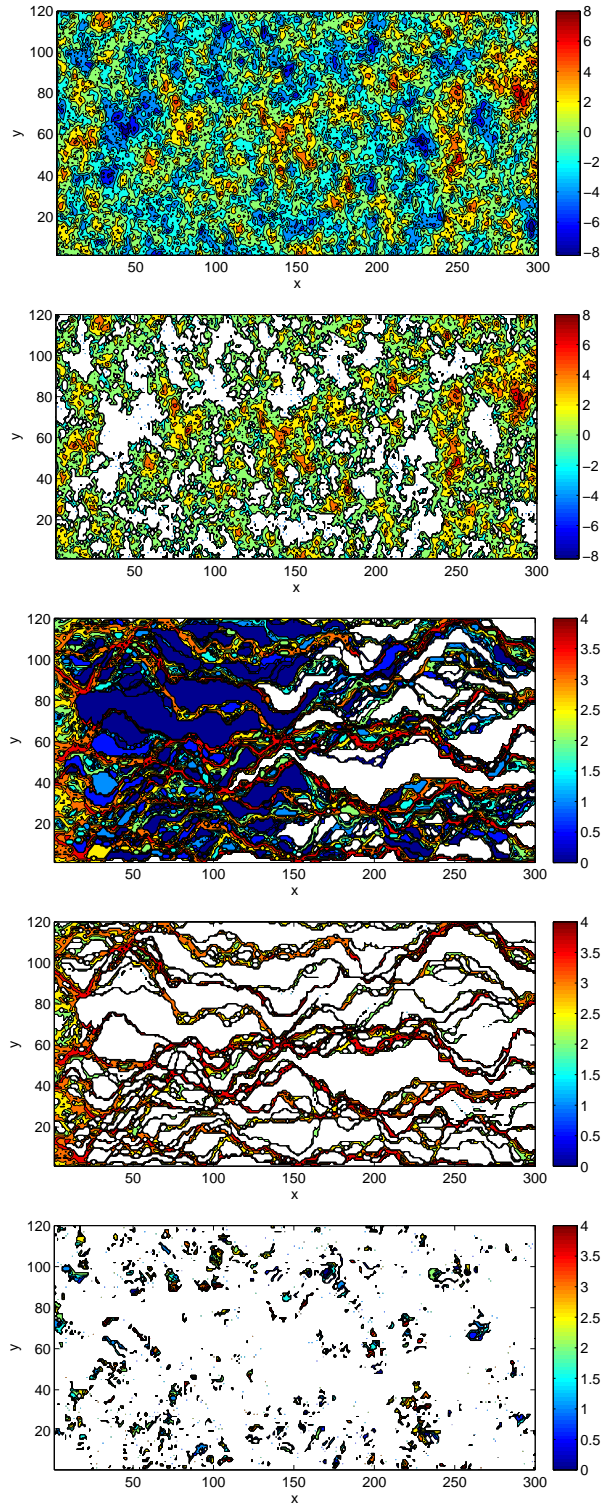


FIG. 2: (Color online) Spatial maps showing (a) full  $K$  field, (b) CPA ( $\ln(K) < -1.13$ ), (c) particle paths, (d) preferential particle paths, defined as paths through cells that each contain a visitation of a minimum of 100 particles ( $= 0.1\%$  of the total number of particles in the domain), (e) “LCT jumps” (see text). Note that the color bars are in  $\ln(K)$  scale for (a)-(b), and log number of particles for (c)-(e).

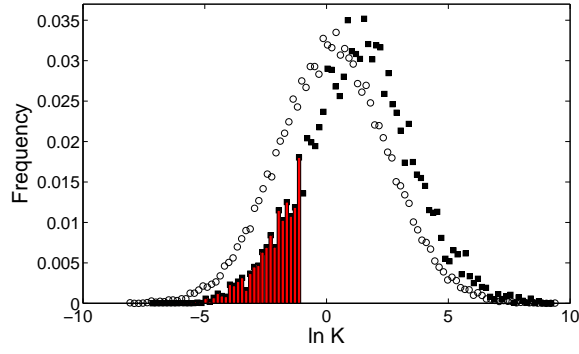


FIG. 3: (Color online) Conductivity histogram normalized by the number of cells (open circles), corresponding to Fig. 2a, with mean  $\ln(K)$  of 0.26 and skewness of 0.03. Conductivity histogram of the preferential particle paths (filled squares) (see Fig. 2c), weighted and normalized by the number of particles visiting in each conductivity cell,  $\{wK\}$ ; with weighted mean of 1.43 and skewness is 3.89. Bars (denoted in red) indicate the frequency of LCT (see Fig. 2e) in the weighted histogram of the preferential particle paths.

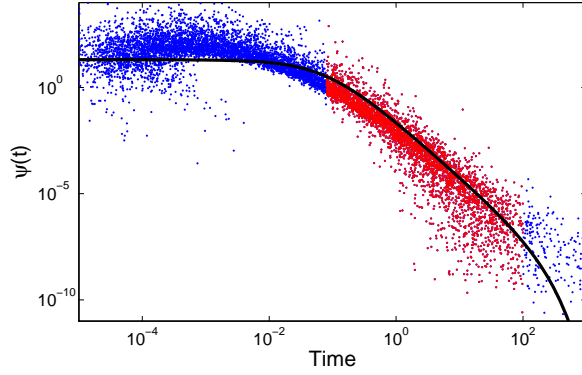


FIG. 4: (Color online) Ensemble particle-weighted conductivity histogram ( $\sigma^2 = 5$ ) for 100 realizations (points), based on histograms such as shown in Fig. 3, yielding a particle transition time distribution within cells, representing  $\psi(t)$  vs.  $t$ . The solid curve shows the TPL (2) with  $\beta = 1.63$ ,  $t_1 = 0.08$ ,  $t_2 = 10^2$ , identical to the values for the fit shown in Fig. 1. Highlighted (in red online) is the power-law region  $t_1 < t < t_2$  corresponding to  $-7.5 < \ln(K) < -1$ .

# Supplementary Material

## Origins of Anomalous Transport in Disordered Media: Structural and Dynamic Controls

Yaniv Edery<sup>1</sup>, Harvey Scher<sup>1</sup>, Alberto Guadagnini<sup>2</sup> and Brian Berkowitz<sup>1</sup>

1. *Department of Environmental Sciences and Energy Research,*

*Weizmann Institute of Science, 76100 Rehovot, Israel*

2. (a) *Dipartimento di Ingegneria Civile e Ambientale,*

*Politecnico di Milano, 20133 Milano, Piazza L. Da Vinci 32,*

*Italy (b) Department of Hydrology and Water Resources,*

*University of Arizona, Tucson, Arizona 85721, USA*

We provide details of the model construction and particle tracking methods, and the derivation of Eq. (4), employed in the main text.

### MODEL CONSTRUCTION AND PARTICLE TRACKING METHODS

Deterministic head values are prescribed along the left and right boundaries of the 2D domain ( $300 \times 120$  cells of uniform length and width  $\Delta = 0.2$ ; all quantities are given in consistent units) while the top and bottom boundaries are impervious. Values of  $\ln(K)$  in each cell are set equal to those generated through a widely tested sequential Gaussian simulator [1]. We generate different random realizations of statistically homogeneous and isotropic, multivariate Gaussian fields. Each field is associated with a spatial covariance of the simple exponential type, with unit correlation length,  $\mathcal{L} = 1$ , and  $\ln(K)$  variance,  $\sigma^2$ . Different values of  $\sigma^2$  are analyzed, to explore fields associated with mildly to strongly heterogeneous conditions. In all scenarios,  $\mathcal{L}/\Delta = 5.0$ , to accurately reproduce the adopted covariance model for  $\ln(K)$  at all spatial lags of interest and its influence on transport [e.g., [2, 3]]. For each generated  $\ln(K)$  field, we solve the corresponding deterministic flow problem using Galerkin finite elements to obtain head and velocity distributions.

Solute movement in each realization is modeled by a Lagrangian particle tracking method, to generate the BTCs. Particles are injected, flux-weighted, along the left boundary. Starting from a known location of the particles at time  $t_k$ , the displacement vector  $\mathbf{d}$  for each particle is given by the Langevin equation

$$\mathbf{d} = \mathbf{v}[\mathbf{x}(t_k)] \delta t + \mathbf{d}_D \quad (1)$$

with  $\mathbf{v}$  the fluid velocity,  $\delta t$  the time step magnitude, and  $\mathbf{d}_D$  the diffusive displacement;  $\xi$  is a  $N[0, 1]$  random number and the modulus of  $\mathbf{d}_D$  is  $\xi\sqrt{2D\delta t}$ . The advective displacement in (1) is computed with the velocity at  $\mathbf{x}$ . A uniform spatial step,  $\delta s$ , along each particle trajectory is fixed. Preliminary numerical tests confirmed that using  $\delta s = \Delta/10$  did not introduce numerical dispersion [4], and that consideration of  $10^5$  particles was sufficient. The magnitude of the time step  $\delta t$  in (1) is calculated as  $\delta t = \delta s/v$ ,  $v$  being the modulus of  $\mathbf{v}$ . Reflection bound-

ary conditions are imposed at no-flow boundaries.

### DERIVATION OF EQUATION (4)

The weighted histogram  $\{wK\}$  is fit by a probability distribution, which is then converted to time with  $K_{ij} = \theta\Delta x^2/\Delta h_{ij}\Delta t$ , which we write as  $K = C/t$  with the understanding that the time associated with each  $K$  is the transit time across a “ $K$ -bin”.

The mean of the data in Fig. 4 can be plotted as

$$f = n_k \frac{\exp(-(\ln K - \mu)^2/2\sigma^2)}{t} \quad (2)$$

where  $\mu$ , the mean of  $\{wK\}$ , is a function of  $\sigma^2$  and the variance of  $\{wK\}$  is  $\approx \sigma^2$ ;  $n_k$  is a normalization constant.

We compute the logarithmic derivative of (2),  $d \log f / d \log t$ . First, we have

$$\log f = \log n_k + \frac{-(\ln K - \mu)^2}{2\sigma^2} \log(e) - \log t. \quad (3)$$

Then

$$d \log f / d \log t = \frac{(\ln K - \mu)}{\sigma^2} \log(e) \ln(10) - 1 \quad (4)$$

so that

$$d \log f / d \log t = \frac{(\ln K - \mu)}{\sigma^2} - 1 \quad (5)$$

because

$$\log(e) \ln(10) = 1. \quad (6)$$

The above is equated to  $-1 - \beta$ , the log derivative of the TPL in the power law region, to obtain

$$\beta = \frac{(\mu - \ln K)}{\sigma^2} \quad (7)$$

which is  $> 0$ .

The result in (7) has a slow time dependence for  $\beta$ . In Fig. 4 there is some curvature in the power-law region. The value for  $\beta$  is determined near the end of the range of small  $\ln(K)$  (large time).

---

- [1] J. J. Gómez-Hernández and A. G. Journel, *Geostatistics Troia'92*, Kluwer Academic Publishers, Dordrecht, Netherlands **1**, 85 (1993).
- [2] R. Ababou, D. McLaughlin, L. W. Gelhar, and A. F. B. Thompson, *Transp. Porous Med.* **4**, 549 (1989).
- [3] M. Riva, A. Guadagnini, and X. Sanchez-Vila, *Math. Geosci.* **41**, 835 (2009).
- [4] C. Cordes and W. Kinzelbach, *Water Resour. Res.* **28**, 2903 (1992).